Arch. Mech., **55**, 5–6, pp. 449–479, Warszawa 2003

Finite element analysis and design optimization of rubber components for vibration isolation

WAN-SUL LEE, SUNG-KIE YOUN and BONG-KYU KIM[1]

Department of Mechanical Engineering,
Korea Advanced Institute of Science and Technology,
373-1, Gusung-dong, Yusung-gu, Daejeon, 305-701, Korea
e-mail:skyoun@sorak.kaist.ac.kr

[1] *R&D Division for Hyundai Motor Company & Kia Motor Corporation,*
Jangduk-dong, Whasung-si, Gyunggi-do, 445-706, Korea

A CONSTITUTIVE THEORY, finite element formulation and topology optimization for anti-vibration rubber are presented. Many vibration isolators made of rubbers are operating under small oscillatory load superimposed on large static deformation. A viscoelastic constitutive equation for rubber is proposed considering the influence of large static pre-deformation on the dynamic properties. The proposed model is derived through linearization of Simo's viscoelastic constitutive model and introduction of static deformation correction factor. And then the model is implemented in a finite element code to analyze the behavior of rubber elements under general loading conditions. Dynamic tests are performed in order to verify the model under multiaxial deformation. The computed results by the FEA code are compared with the experimental results and the suggested constitutive equation with static deformation correction factor shows good agreement with the test values. For the stability and low transmissibility of isolation systems, both static and dynamic performance must be concurrently considered in the design process. The continuum-based design sensitivity analyses (DSA) of both the static hyperelastic model and dynamic viscoelastic model are developed. And then the topology optimization methodology is used in order to generate the system layouts considering both the static and dynamic performance.

1. Introduction

MANY RUBBER COMPONENTS, which are used as vibration isolators, experience small oscillatory loads superimposed on large static deformation. Most of dynamic properties of vibration isolators can be described by linearized steady-state harmonic response. Considering nonlinear behavior of rubber under large deformation, it is evident that even linearized dynamic properties depend heavily on prestrain. The accurate constitutive equation that describes rubber under the loading conditions is essential in analyzing the dynamic behavior of rubber and designing the shape of rubber elements.

http://rcin.org.pl

Morman's model is widely used to describe viscoelastic behavior of rubber that is under small oscillatory loads superimposed on large static deformation [1–5]. Morman derived a viscoelastic constitutive model from the assumption that the time effect and large prestrain effect can be separable. The separability assumption leads to simple relaxation function that is independent of deformation. It is observed in experiments that the separability assumption is applicable to unfilled rubber [1, 6]. In filled rubber, however, the relaxation function is a function of prestrain [6, 7]. Rubber is seldom used as pure gum, because addition of fillers to elastomers improves mechanical properties [8]. Therefore it is very important to consider the effects of prestrain in the constitutive theory of small viscoelastic motion superimposed on large static deformation in many engineering rubber materials [9].

In the previous work [9], the authors have proposed Linearized Simo's Viscoelastic Model (LSVM) with static deformation correction factor as a constitutive equation of rubber that is under small oscillatory loads superimposed on large static deformation. In this constitutive model, the statically pre-deformed configuration has been used as the reference configuration. And static deformation correction factor has been introduced to consider the influence of prestrain on the relaxation function. In the previous work, it has been observed that the proposed model works well under single stress component.

In this work, the proposed model is implemented in a finite element code that enables us to predict the behavior of rubbers for general complex shapes and loading conditions. And dynamic tests are executed in order to verify the proposed constitutive model. Complex stress-state tests are included in the dynamic tests in order to assure the proposed model under multi-axial stress states. The computed results by the FEA code are compared with the experimental results in order to estimate the performance of the model.

Many works for engine mount system of vehicles and aircrafts used two-level design approaches [10]. First step is the system level design in order to decide the mounting location and mount stiffness. In this level, simple spring-damper models are generally used with constant parameters such as dynamic-to-static ratio and loss factor. However these models are too simple to describe the complex behavior of rubber-like materials. Second step is the isolator shape design to get target stiffness decided in the first step. Various optimization approaches [11–13] are applied to the shape design, but they consider the only static hyperelastic behavior of rubber. Most vibration isolators must endure the static loadings due to large gravitational and inertial forces. And also they must be dynamically flexible in order to have small natural frequencies and reduce the transmitting dynamic force from the vibrating systems to the other structures. Therefore in the stiffness and shape design process of the vibration isolators, both static and dynamic behavior of rubber materials must be

http://rcin.org.pl

simultaneously considered for the structural stability and the vibration isolation.

For the stability and low transmissibility of isolation systems, both static and dynamic performance must be concurrently considered in the design process. Among the various design methods, a topology optimization approach can be applied for the shape design of vibration isolator made of filled rubber. For easier application of the optimization algorithm, two kinds of continuum-based design sensitivity analysis method are developed. Material property design sensitivity analysis of both the hyperelastic constitutive equation and the steady-state viscoelastic one are developed for topology optimization using the mean compliance and adjoint variables. In order to consider simultaneously the static and dynamic behavior of rubber, a proper topology optimization formulations is proposed.

2. Constitutive equation and FE formulation

2.1. Notation

The small deformation superimposed on the large static deformation is depicted in Fig. 1. Let Φ_ξ denote the configuration of the body $\mathscr{B}$ at instant ξ. Configuration $\Phi_{t'}$, Φ_{t_0} and Φ_t refer respectively to the undeformed, the statically deformed and the current configuration. ${}_\xi T(\eta)$ represents a tensor T at time η with respect to a configuration Φ_ξ. For convenience, the following simplified notations are also used:

$$T(\eta) = {}_{t'}T(\eta), \qquad {}_\xi T_0 = {}_\xi T(t_0), \qquad {}_0T(\xi) = {}_{t_0}T(\xi), \qquad {}_\xi T = {}_\xi T(t). \tag{2.1}$$

The deformation gradient and volume preserving deformation gradient tensor are denoted by

$$({}_\xi F(t))_{ij} = \left(\frac{\partial x_i(t)}{\partial X_j(\xi)}\right), \qquad {}_\xi\overline{F} = J^{-1/3}{}_\xi F, \tag{2.2}$$

where J is $\det({}_\xi F)$. Left and right Cauchy–Green tensors that correspond to ${}_\xi\overline{F}$ and ${}_\xi F$ are

$${}_\xi C = {}_\xi F^T {}_\xi F, \qquad {}_\xi\overline{C} = {}_\xi\overline{F}^T {}_\xi\overline{F}, \tag{2.3}$$

$${}_\xi B = {}_\xi F {}_\xi F^T, \qquad {}_\xi\overline{B} = {}_\xi\overline{F} {}_\xi\overline{F}^T \tag{2.4}$$

and Green strains are defined by

$${}_\xi E = \frac{1}{2}\left({}_\xi C - I\right), \qquad {}_\xi\overline{E} = \frac{1}{2}\left({}_\xi\overline{C} - I\right). \tag{2.5}$$

http://rcin.org.pl

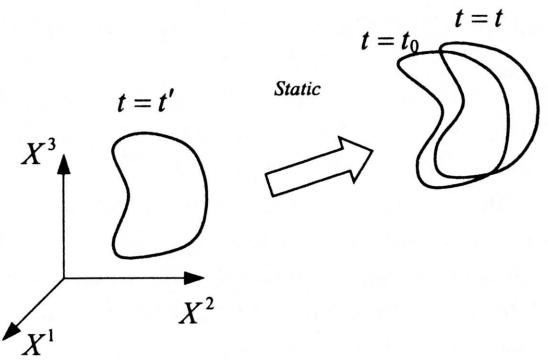

FIG. 1. Large static deformation + small dynamic deformation.

2.2. Linearized Simo's viscoelastic model (LSVM)

Simo proposed a finitely deformable viscoelastic model from the generalization of standard linear solid model [14]. The characteristics of Simo's model are decoupled bulk and deviatoric responses over any range of deformations and linear rate constitutive equation. Simo's nonlinear viscoelastic constitutive model is written as follows:

$$S = JC^{-1}\frac{\partial U}{\partial J} + J^{-2/3}\mathrm{DEV}\left[\left(\frac{\partial \Psi}{\partial \overline{E}}\right)\right] + J^{-2/3}\mathrm{DEV}\left[\int_0^t g(t-\xi)\frac{\partial}{\partial \xi}\mathrm{DEV}\left(\frac{\partial \Psi}{\partial \overline{E}}\right) d\xi\right], \tag{2.6}$$

where $\mathrm{DEV}[\bullet] = (\bullet) - 1/3\,[C : (\bullet)]\; C^{-1}$, U and Ψ are the volumetric and deviatoric parts of the elastic free energy function. From this model, static stress is given as

$$\sigma_0 = P_0 I + \mathrm{dev}\,[\widehat{\sigma}_0], \tag{2.7}$$

where $P_0 = \dfrac{\partial U}{\partial J}$, $\widehat{\sigma}_0 = \dfrac{1}{J}\overline{F}_0\dfrac{\partial \Psi}{\partial \overline{E}}\overline{F}_0^T$ and $\mathrm{dev}\,[\bullet] = (\bullet) - 1/3\,[I : (\bullet)]\, I$. We know from the above equation that static behavior of Simo's model is exactly equal to that of hyperelastic material. The static stress caused by prestrain is determined only by the last state of static deformation. Because of the fading memory hypothesis [15, 16] of the viscoelastic material, the effects of the deformation history are relaxed out. Thus we can assume that viscoelastic effects depend only on the superimposed small vibratory deformation.

A linearized constitutive equation that specifies the behavior of rubber under small oscillatory load superimposed on large static deformation can be derived

http://rcin.org.pl

from the assumption that the superimposed motion is small. Repeated applications of the chain rule to Eq. (2.6) and the reference configuration transformation yield the relation between the stress increment $\Delta_0 S$ and the superposed strain increment ε.

$$\Delta_0 S = \left(J\frac{\partial^2 U}{\partial J^2} + P\right)\varepsilon_{kk} I - 2P\varepsilon - \frac{2}{3}\left[\operatorname{dev}(\widehat{\sigma}_0)\otimes I + I\otimes \operatorname{dev}(\widehat{\sigma}_0)\right] : \varepsilon + \mathscr{C} : \varepsilon + \int_0^t g(t-\xi)\,\mathscr{C} : \dot{\varepsilon}\, d\xi, \tag{2.8}$$

$$\mathscr{C} = \frac{2}{3}\left(\widehat{\sigma} : I\right)\left(\widehat{I} - \frac{1}{3} I\otimes I\right) + \mathscr{F} - \frac{1}{3}\left[(\mathscr{F} : I)\otimes I + I\otimes(\mathscr{F} : I)\right] + \frac{1}{9}(I : \mathscr{F} : I)\, I\otimes I, \tag{2.9}$$

where $\mathscr{F}_{ijkl} = \dfrac{1}{J}\overline{F}_{iI}\overline{F}_{jJ}\overline{F}_{kK}\overline{F}_{lL}\left(\dfrac{\partial^2 \Psi}{\partial \overline{E}^2}\right)_{IJKL}$ and $\widehat{I}$ is the fourth order identity tensor.

Let us suppose that the superimposed deformation is steady-state harmonic such as $\varepsilon = \varepsilon^* e^{i\omega t}$. Then the complex constitutive relation is extracted from Eq. (2.8).

$$\Delta_0 S^* = \left(J\frac{\partial^2 U}{\partial J^2} + P\right)\varepsilon^*_{kk} I - 2P\varepsilon^* - \frac{2}{3}\left[\operatorname{dev}(\widehat{\sigma})\otimes I + I\otimes \operatorname{dev}(\widehat{\sigma})\right] : \varepsilon^* + (1 + i\omega g^*)\,\mathscr{C} : \varepsilon^*, \tag{2.10}$$

where g^* is the Fourier transform of $g(t)$ i.e. $g^*(\omega) = \int_0^\infty g(t)\, e^{-i\omega t} dt$. The relation between g^* and complex shear modulus $G^* = G' + iG''$ is as follows:

$$\omega g^* = \frac{G''}{G_\infty} + \left(1 - \frac{G'}{G_\infty}\right) i. \tag{2.11}$$

2.3. Static deformation correction factor

Thus far it has been assumed that $g(t)$, which represents the time effects, is not affected by static deformation. This separability assumption of time and large prestrain is suitable for the rubbers that do not contain such fillers as carbon black [6, 7]. However, it is known from experiments that $g(t)$ depend

http://rcin.org.pl

on the static deformation for filled rubber [6]. Unfilled rubber is seldom used for engineering applications, because the addition of fillers improves their mechanical properties [8]. Therefore the influences on $g(t)$ due to the static deformation must be considered in order to develop a realistic viscoelastic constitutive model. In order to describe the non-separability nature of filled rubber, we introduce a static deformation correction factor $c^*(B_0)$ to the constitutive equation. Now we define $\widehat{g}^*$ which is the correction of $1 + i\omega g^*$ in Eq. (2.10).

$$\widehat{g}^* = (1 + i\omega g^*)\, c^*(B_0), \tag{2.12}$$

where $c^*(B_0)$ is a complex-valued function that depends on the static deformation. $\widehat{g}^*$ can also be described as follows using complex shear modulus and $c^*(B_0)$.

$$\widehat{g}^*(\omega, B_0) = \frac{G^*(\omega)}{G_\infty} c^*(B_0) = \left(\frac{G'}{G_\infty} + i\frac{G''}{G_\infty}\right) c^*(B_0) = \frac{\widehat{G}^*}{G_\infty}. \tag{2.13}$$

In the above equation, $\widehat{G}^*$ can be interpreted as an effective complex shear modulus under static deformation. The static deformation correction factor can be expressed by the modulus and argument of c^*,

$$c^*(B_0) = c\, e^{i\theta}. \tag{2.14}$$

To define c^* in a specific form, we need to measure the static deformation that is described by the tensor B_0. It is observed that generalized octahedral shear strain has good performance as a static deformation measure. The generalized octahedral shear strain [17] is defined as

$$\overline{I}_\gamma = \frac{1}{6}\left(2\overline{I}_1^2 - 6\overline{I}_2\right)^{1/2}, \tag{2.15}$$

where $\overline{I}_1$ and $\overline{I}_2$ are the first and second invariants of the right Cauchy–Green tensor $\overline{C}$. $\overline{I}_\gamma$ is an invariant of B_0 and represents the octahedral shear strain under infinitesimal deformation. Since the value of c^* is unity without the static deformation, the following polynomial forms can serve as the static deformation correction factors:

$$c_\gamma^*(\overline{I}_\gamma) = c_\gamma e^{i\theta_\gamma}, \tag{2.16}$$

$$c_\gamma(\overline{I}_\gamma) = 1 + z_{\gamma_1}\overline{I}_\gamma + z_{\gamma_2}\overline{I}_{\gamma^2}, \tag{2.17}$$

$$\theta_\gamma(\overline{I}_\gamma) = {}_\theta z_\gamma \overline{I}_\gamma, \tag{2.18}$$

where z_{γ_1}, z_{γ_2} and ${}_\theta z_\gamma$ are material constants. The material constants can be easily determined by the results of uniaxial tension test.

http://rcin.org.pl

2.4. Mixed FE formulation of static deformation

For the FEA of a rubber element that is under small steady-state dynamic load superimposed on large static deformation, the static analysis results such as statically deformed shape and static stress state are required. Since rubber can be idealized as a hyperelastic material as mentioned in the previous section, static deformation analysis results can be easily obtained using the techniques that are developed for the FEA of hyperelastic material. In the static analysis, nonlinearity due to large deformation and incompressibility characteristics of rubber should be effectively treated, and so the updated Lagrangian formulation with displacement-pressure mixed method (u/p mixed method) is used in this paper.

The mixed finite element formulation that was proposed by SUSSMAN and BATHE [18] is used in order to analyze the incompressible large deformation problems. In the mixed method, pressure that is defined by $-\sigma_{kk}/3$ is independent of the displacement field and interpolated by its own shape function. The independent pressure variable is denoted by $\widehat{p}$ and the pressure computed from displacement is represented by $\overline{p}$. By definition of pressure and Eq. (2.7), $\overline{p}$ has the following description:

$$\overline{p} = -\frac{\partial U}{\partial J}. \tag{2.19}$$

The stress is composed of the derivatives of the strain energy function that is obtained from the displacement field and the independent pressure field.

$$ {}_0S(t_0) = \sigma(t_0) = \frac{1}{J_0}\mathrm{dev}\left[\overline{F}_0 \frac{\partial \Psi}{\partial \overline{E}} \overline{F}_0^T\right] - \widehat{p}I. \tag{2.20}$$

The governing equations in the u/p mixed method are described by the following weak forms:

$$\int_V \left(\frac{\partial_0 W}{\partial_0 E} - \frac{1}{KJ_0}(\overline{p} - \widehat{p})\frac{\partial \overline{p}}{\partial_0 E}\right) : \delta_0 E \, dV = \int_V {}_0S : \delta_0 E \, dV = \Re, \tag{2.21}$$

$$\int_V \frac{1}{KJ_0}(\overline{p} - \widehat{p})\,\delta\widehat{p}\, dV = 0. \tag{2.22}$$

In the above equations, the first and second equations are respectively the equilibrium equation and pressure constraint between $\widehat{p}$ and $\overline{p}$. $\Re$ and K represent the external virtual work and bulk modulus of rubber, respectively. ${}_0W$ that

http://rcin.org.pl

is the strain energy per unit volume of statically deformed state is defined as follows:

$$ {}_0W = \frac{\widehat{\Psi}}{J_0} = \frac{1}{J_0}\left(\Psi + U\right). \tag{2.23} $$

In this paper, U and Ψ are described by the Mooney–Rivlin model and the second order polynomial of J. The specific form of the strain energy function is

$$ \Psi = c_1\left(\overline{I}_1 - 3\right) + c_2\left(\overline{I}_2 - 3\right), \tag{2.24} $$

$$ U = \frac{1}{2}K\left(J-1\right)^2, \tag{2.25} $$

where c_1, c_2 and bulk modulus K are the material constants of rubber.

The solution of the governing equations cannot be obtained directly because the equations are nonlinear. Thus we use the Newton–Raphson method in which the linearized governing equations are solved by the iterative technique. The incremental form of the governing equation can be written as follows:

$$ \int_V \delta\varepsilon : \left[\mathscr{D} - \widehat{p}\left(I\otimes I - 2\widehat{I}\right)\right] : \varepsilon \, dV + \int_V \sigma_0 : \Delta\delta_0 E \, dV + \int_V -\Delta\widehat{p}I : \delta\varepsilon \, dV = \Re - \int_V \sigma_0 : \delta\varepsilon \, dV, \tag{2.26} $$

$$ \int_V -\delta\widehat{p}I : \varepsilon dV - \int_V \frac{1}{KJ_0}\delta\widehat{p}\Delta\widehat{p} \, dV = -\int_V \frac{1}{KJ_0}\left(\overline{p}_0 - \widehat{p}_0\right)\delta\widehat{p}\, dV, \tag{2.27} $$

where $\delta\varepsilon_{ij} = \frac{1}{2}\left(\frac{\partial\delta u_i}{\partial x_j} + \frac{\partial\delta u_j}{\partial x_i}\right)$ and $\mathscr{D} = \frac{1}{J_0}\frac{\partial^2\Psi}{\partial_0 E\partial_0 E}$. To solve Eqs. (2.26) and (2.27), the displacement and pressure field are approximated by the shape functions.

$$ u_i = N^I u_i^I, \tag{2.28} $$

$$ \widehat{p} = N_p^I \, \widehat{p}^I. \tag{2.29} $$

In the above equations, N^I is the interpolation function for the displacement and N_p^I is the interpolation function for pressure. u_i^I is the displacement at the I-th node in the i direction and $\widehat{p}^I$ is the I-th pressure degree of freedom. The element used in this study has 27 displacement nodes and 4 pressure degrees

http://rcin.org.pl

of freedom. The interpolation function for displacement field is the conventional isoparametric shape function that continuously interpolates the field between elements. The pressure field is interpolated by a linear polynomial using element local coordinates and it is discontinuous between elements. Using finite element approximation, the governing incremental equations are converted to the following matrix equation:

$$\begin{bmatrix} K_{UU} & K_{UP} \\ K_{PU} & K_{PP} \end{bmatrix} \begin{Bmatrix} \Delta u \\ \Delta \hat{p} \end{Bmatrix} = \begin{Bmatrix} \mathscr{R} \\ 0 \end{Bmatrix} - \begin{Bmatrix} F_U \\ F_P \end{Bmatrix}, \tag{2.30}$$

where K_{UU}, K_{UP}, K_{PP}, F_U and F_P are defined as follows:

$$(K_{UU})_{mn} = \int \frac{\partial \varepsilon_{ij}}{\partial u_r^I} \left[\mathscr{D} - \hat{p} \left(I \otimes I - 2\hat{I} \right) \right]_{ijkl} \frac{\partial \varepsilon_{kl}}{\partial u_s^J} \, dV + \int \sigma_{ij} \frac{\partial^2 {}_0E_{ij}}{\partial u_r^I \partial u_s^J} \, dV, \tag{2.31}$$

$$(K_{UP})_{mq} = (K_{PU})_{qm} = -\int \frac{\partial N^I}{\partial x_r} N_p^q \, dV, \tag{2.32}$$

$$(K_{PP})_{qt} = -\int \frac{1}{KJ_0} N_p^q N_p^t \, dV, \tag{2.33}$$

$$(F_U)_m = \int \sigma_{ij} \frac{\partial \varepsilon_{ij}}{\partial \mathrm{u}_\mathrm{r}^I} \, dV, \tag{2.34}$$

$$(F_P)_q = \int \frac{1}{KJ_0} (\bar{p} - \hat{p}) \, N_p^q \, dV. \tag{2.35}$$

In the above equations, m and n denote respectively the displacement degree of freedom at the I-th node in direction r and the J-th node in directions in the global matrix.

2.5. FE formulation of steady-state dynamic deformation superposed on large static deformation

The finite element formulation for the dynamic analysis is easily derived through generalization of the static incremental formulation. In the dynamic formulation, the viscoelastic behavior that alters the stress-strain relation and

http://rcin.org.pl

the inertia effects must be considered. Assuming that the displacement and external force increments which are superimposed on the static deformation are varying in steady-state harmonic manner, the increments are written as follows:

$$\Delta u = \Delta u^* e^{i\omega t}, \quad \Delta \hat{p} = \Delta \hat{p}^* e^{i\omega t}, \quad \Delta \mathscr{R} = \Delta \mathscr{R}^* e^{i\omega t}, \quad \Delta S = \Delta S^* e^{i\omega t}. \tag{2.36}$$

The stress increments are determined by the proposed constitutive equation. Because we use the mixed method in the FEA, the pressures and their increments in the constitutive relations are converted to the independent variables. The stress increments are calculated by

$$\Delta S^* = \mathscr{D}^* : \varepsilon^* - \hat{p}_0 \left(I \otimes I - 2\hat{I} \right) : \varepsilon^* - \Delta \hat{p}^* I, \tag{2.37}$$

where $\mathscr{D}^* = \overset{*}{g}\mathscr{C} - 2/3\,[\mathrm{dev}\,(\hat{\sigma}_0) \otimes I + I \otimes \mathrm{dev}\,(\hat{\sigma}_0)]$. The inertia effects due to dynamic deformation can be regarded as the body force $\rho\omega^2 \Delta u^*$ by d'Alembert's principle. We can obtain directly the dynamic finite element formulation using the same procedure that is used in the previous static case except for the complex constitutive relation and the inertial body force. The finite element matrix equation for a rubber element subject to steady-state harmonic motion superposed on finite static deformation is

$$\begin{bmatrix} M + K^*_{UU} & K_{UP} \\ K^T_{UP} & K_{PP} \end{bmatrix} \begin{Bmatrix} \Delta u^* \\ \Delta \hat{p}^* \end{Bmatrix} = \begin{Bmatrix} \Delta \mathscr{R}^* \\ 0 \end{Bmatrix}. \tag{2.38}$$

In the above equation, the mass matrix and the dynamic stiffness matrix is written as follows:

$$M_{mn} = -\delta_{rs} \int \rho\omega^2 N^I N^J \, dV, \tag{2.39}$$

$$(K^*_{UU})_{mn} = \int \frac{\partial \varepsilon^*_{ij}}{\partial u^{*I}_r} \left[\mathscr{D}^* - \hat{p}_0 \left(I \otimes I - 2\hat{I} \right) \right]_{ijkl} \frac{\partial \varepsilon^*_{kl}}{\partial u^{*J}_s} \, dV + \int \sigma_{ij} \frac{\partial^2 {}_0 E^*_{ij}}{\partial u^{*I}_r \partial u^{*J}_s} \, dV. \tag{2.40}$$

The dynamic stiffness matrix depends on the static prestress and frequency due to the definition of $\mathscr{D}^*$ and Eq. (2.40). Comparing Eqs. (2.30) and (2.38), we see that the steady-state dynamic finite element equation has the same structure as the incremental equation for static deformation, except that the dynamic equation has the mass matrix and the complex stiffness matrix.

http://rcin.org.pl

3. Experiment and prediction by the constitutive model

Dynamic tests in which the rubber specimens are subject steady-state harmonic motion superimposed on large static deformation have been executed in order to verify the proposed constitutive model. The tests performed in this work are composed of the uniaxial tension tests and the complex stress-state tests. The coefficients in the proposed model are determined by uniaxial tension test. The determined coefficients are required in FEA of complex stress-state test to specify the constitutive model. In the previous paper [9] it was observed that the proposed model works well under single stress component. In this paper, the complex stress-state test is carried out to verify the model under multi-axial stress state. Varying the size of static deformation, the dynamic stiffness of each specimen is measured and compared with the predicted value that is calculated by FEM using the proposed model. By comparison of the results, we can verify whether the model effectively describes the behavior of rubber subject to the steady-state harmonic motion superposed on finite static deformation.

The tests have been performed at room temperature (26°C) using a servo-hydraulic rubber tester(Instron-5802). To subject the specimen to small dynamic motions superimposed on finite static deformations, experiments are conducted in two steps. Finite prestrain is applied to each specimen with 20 minutes of relaxation time in order to achieve the static equilibrium. After that, the dynamic load is superimposed on the static deformation. The dynamic displacement amplitude is 0.5% with respect to the deformed specimen length. Initial conditioning has been applied 12 hours in advance before the test. For the initial conditioning, each test specimen is exposed to the highest strain and frequency in the test series in order to remove irreversible material structures [19]. The measurement is executed after 50 cycles of initial dynamic loading. When the test is executed using the displacement-control mode, the dynamic displacements and the corresponding dynamic driving forces are measured as the experiment results. And then from these test data, the dynamic modulus and stiffness can be calculated considering the size of specimens.

Table 1. Recipes of specimens.

Ingredient	Content (phr)	Ingredient	Content (phr)	Ingredient	Content (phr)
NR	100	Carbon black GPF	50	Antidegradant	4
ZnO	3	TBBS	1.0		
Stearic acid	1.0	S	1.75		

http://rcin.org.pl

Table 2. Material constants and the coefficients of static deformation correction factor.

Material constant	Value	Material constant	Value	Material constant	Value
c_1 (MPa)	0.46	ρ (kg/m^3)	1124.7	${}_\theta z_\gamma$	−0.0627
c_2 (MPa)	0.08	$z_{\gamma 1}$	−2.841		
G_∞ (MPa)	1.08	$z_{\gamma 2}$	10.81		

The rubber specimens used in this work are made of natural rubber and other ingredients. The recipes and material constants of the rubber are shown in Table 1 and Table 2. Aluminum plates are bonded to both ends of the rubber specimen by quick setting adhesive and each plate is bolted to the test machine. The pictures of specimens used in uniaxial tension test and complex stress-state test are shown in Fig. 2 and Fig. 3.

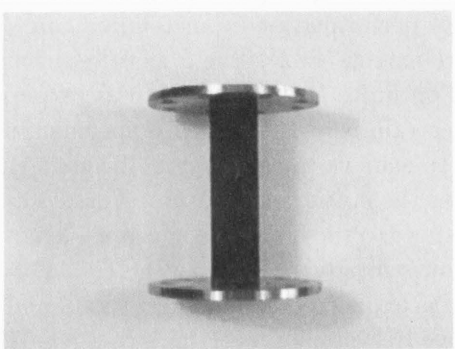

FIG. 2. Tension specimen.

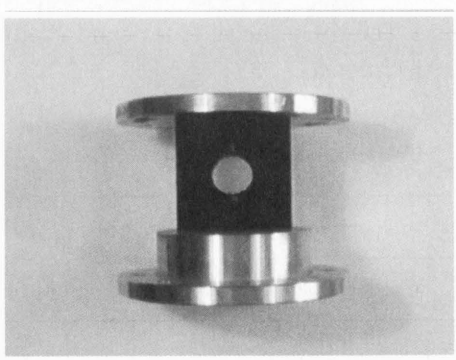

FIG. 3. Complex stress-state specimen.

http://rcin.org.pl

3.1. Uniaxial tension test

Using the uniaxial tension test, the behavior of rubber under tensile loading conditions can be examined and the performance of the proposed constitutive model can be verified by comparing the test results with the calculated results. As a pre-deformation, the static deformation in the range from 0% ($\lambda = 1$) to 30% ($\lambda = 1.3$) is applied to the specimen. The 0.5% dynamic strain amplitude with respect to the deformed specimen length is superimposed on static deformation in $1 \sim 30$ Hz frequency range. The definition of stretch and dynamic strain is as follows:

$$\lambda = \frac{l}{l_0} = \frac{l_0 + \Delta l_0}{l_0} = 1 + \frac{\Delta l_0}{l_0}, \tag{3.1}$$

$$\varepsilon = \frac{\Delta l}{l}. \tag{3.2}$$

In the above equations, l_0, l, Δl_0 and Δl are respectively, the original length of a specimen in the direction of the test machine axis, length of the specimen after static deformation, static displacement and dynamic displacement amplitude.

As results of the dynamic tension test, storage and loss modulus of the specimen are shown in Fig. 4 and Fig. 5 as a function of vibrating frequency for each static tension case. The well-known near-linear relation between the stiffness and log frequency is observed under different static deformation. We also can observe that the dynamic stiffness is moved vertically with static deformation and conclude that the frequency effect is not influenced by static deformation. In order to

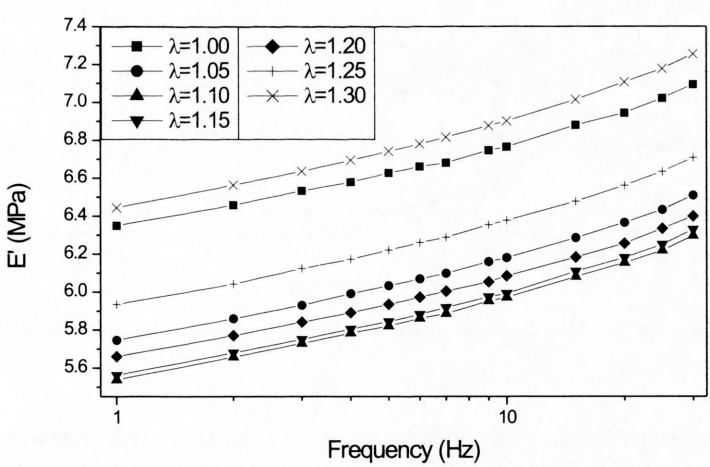

FIG. 4. Storage modulus against frequency at different static stretch for uniaxial tension specimen.

http://rcin.org.pl

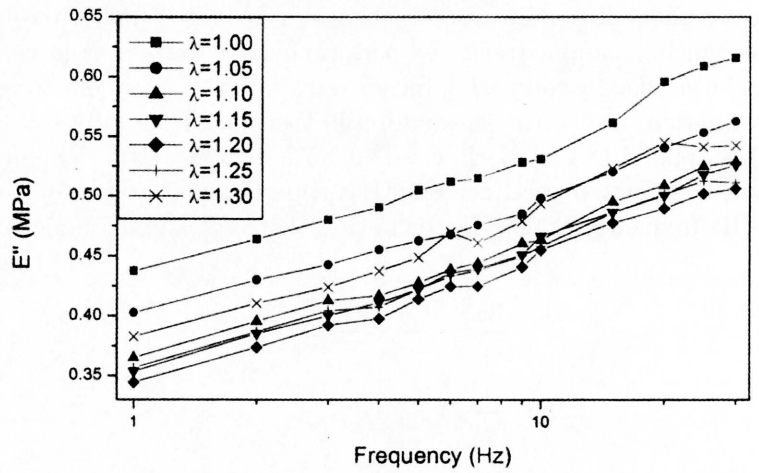

FIG. 5. Loss modulus against frequency at different static stretch for uniaxial tension specimen.

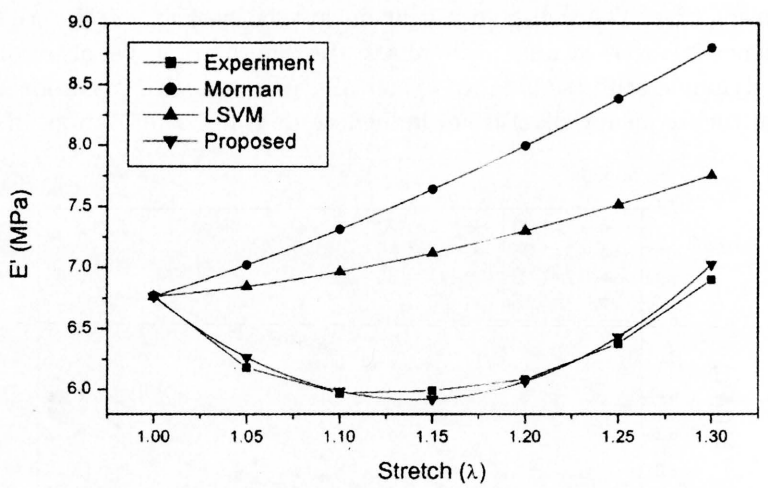

FIG. 6. Storage modulus against static stretch at 10 Hz for the uniaxial tension test.

estimate the performance of the constitutive equation, the measured dynamic modulus and thecalculated ones are plotted at 10 Hz with respect to static deformation in Fig. 6 and Fig. 7. The proposed model successively describes the effects of static deformation. It is observed that the complex Young's modulus

http://rcin.org.pl

of rubber shows an initial decrease followed by an increase with enlargement of static stretch in the uniaxial tension test. In the uniaxial tension test, Morman's model and LSVM in which static deformation effects are not considered, cannot describe the variation of the modulus by static stretch. The proposed model describes properly the dynamic behavior of the rubber. The constitutive equations in which static deformation effects are not considered tend to predict higher dynamic stiffness than the value measured in the compression test.

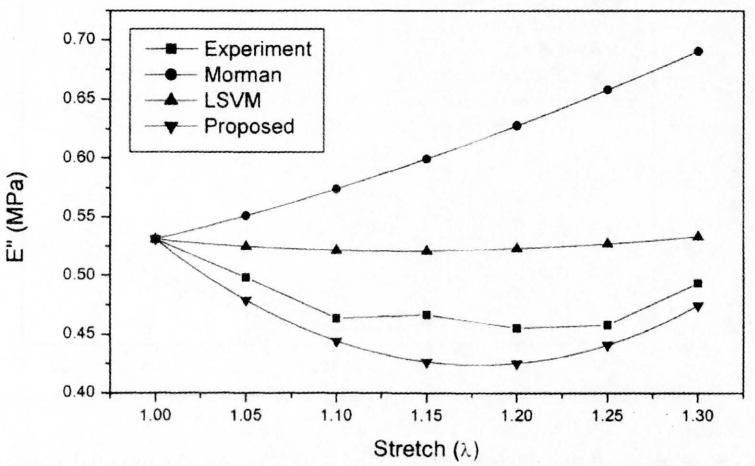

FIG. 7. Loss modulus against frequency at different static stretch for uniaxial tension specimen.

In the prediction of loss modulus, the proposed model anticipates smaller value than the measured result but shows a similar trend. Since the loss moduli are very small compared with the storage modulus and are very sensitive to experimental condition, consistent experiments are difficult to be performed for the loss moduli. The differences between the computed values and the measured ones could be caused by these difficulties. However, the dynamic moduli calculated by the proposed model show the trends of initially decreasing and gradually increasing against the static deformations, as similarly shown in the experimental results.

The storage modulus is plotted with respect to the static deformation at frequencies 5 Hz and 30 Hz in Fig. 8 and Fig. 9. In these figures we can observe that the proposed constitutive model works well at other frequencies. The value of c^* used in the analysis at frequencies 5 Hz and 30 Hz is determined by the uniaxial tension test results at 10 Hz. This means that the static deformation correction factor determined at one frequency is effective at other frequencies in

http://rcin.org.pl

the tested range. This confirms authors' assumption that c^* is only a function of static deformation.

By the discussion given in this section, the constitutive model proposed in this work efficiently describes the effects of static deformation and shows better performance than the conventional constitutive model in predicting the dynamic behaviors of rubber specimens subject to large static deformations.

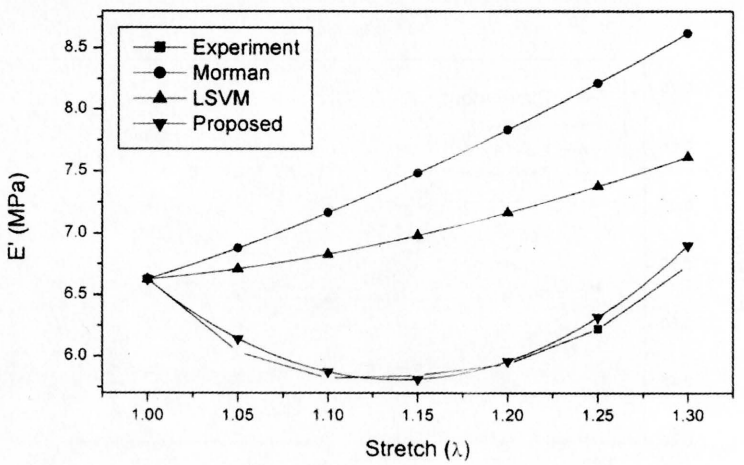

FIG. 8. Storage modulus against static stretch at 5 Hz for the uniaxial tension test.

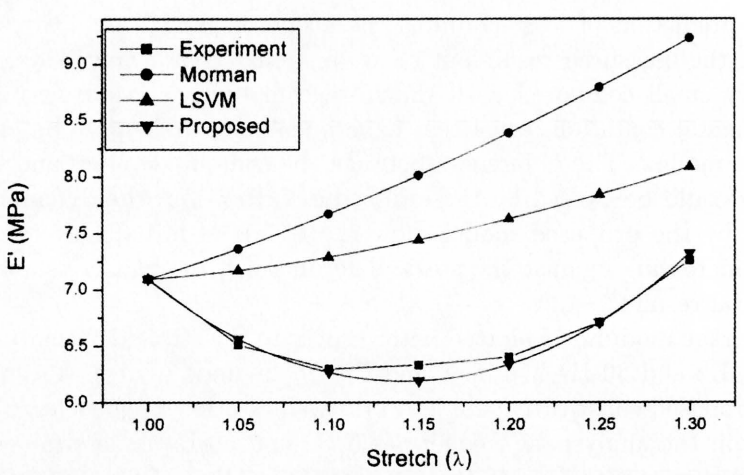

FIG. 9. Storage modulus against static stretch at 30 Hz for the uniaxial tension test.

http://rcin.org.pl

3.2. Complex stress-state test

Complex stress-state test in which the specimens are under more complicated stress state is used to verify the proposed constitutive model. The specimen used in this test has the shape of a hexahedral block with a central hole and is under intricate stress state when it is deformed as shown in Fig. 10 and Fig. 11. The static deformations are applied to the specimen and the values of deformations are in the range from 15% compression ($\lambda = 0.85$) to 20% tension ($\lambda = 1.2$). The 0.5% dynamic strain amplitude with respect to the deformed specimen length was superimposed on the static deformation over $1 \sim 30$ Hz frequency range. Varying the magnitude of static deformation, the dynamic stiffness defined by the following equation is measured and compared with the computed result:

$$K^* = K' + iK'' = \frac{\Delta F^*}{\Delta l^*}, \tag{3.3}$$

where ΔF^* and Δl^* are the dynamic force and displacement.

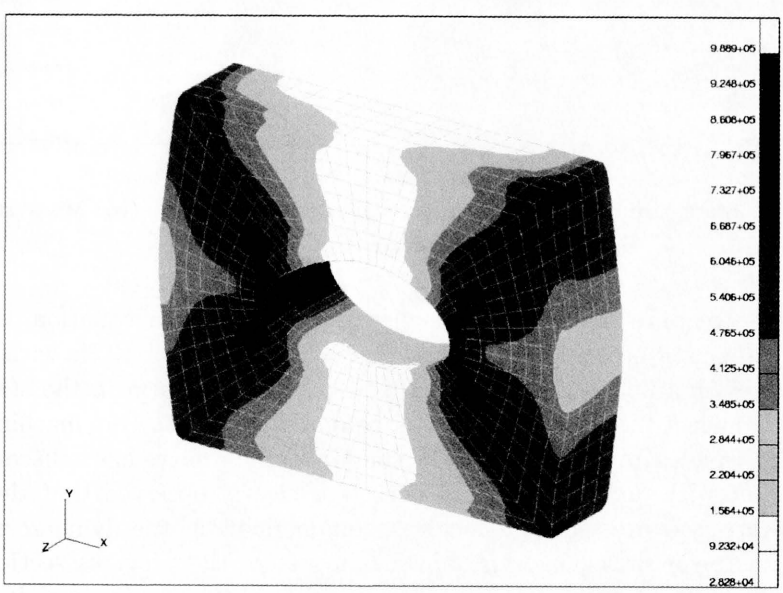

FIG. 10. Static stress distribution for the complex stress specimen (von Mises' stress, $\lambda = 0.85$).

From the results of complex stress-state test, the relations between dynamic stiffness and frequency for each static deformation show the nearlinear relation. This trend is very similar with uniaxial tension test results shown in Fig. 4 and Fig. 5. The dynamic stiffness moves upwards with static compression and

http://rcin.org.pl

downwards with static tension. The effective cross-sectional area of the specimen increases with the compression and decreases with the tension, as shown in Fig. 10 and Fig. 11.

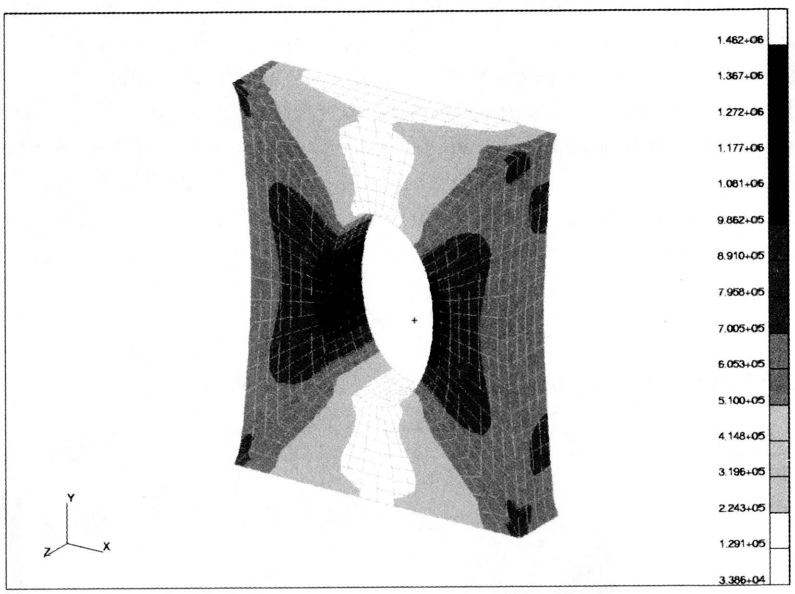

FIG. 11. Static stress distribution for the complex stress specimen (von Mises' stress, $\lambda = 1.20$).

In order to appreciate the performance of the constitutive equation, the measured dynamic stiffness and the calculated one are plotted at 10 Hz with respect to static deformation in Fig. 12 and Fig. 13. The minus sign in the static displacement means that the specimen is compressed by the test machine. It is interesting to notice that the slope of dynamic stiffness curve has a discontinuity at the point with no static deformation. It is clearly observed that the undeformed state is expressed as a local maximum point in the dynamic stiffness plot. It has been shown in uniaxial tension test of the previous section, that the modulus of rubber decreases with static deformation in the vicinity of the undeformed state. The dynamic stiffness of complex stress-state test specimen is decreased by both pre-applied tension and compression pre-deformation. Thus the dynamic test results have a peak when the specimen is under no prestrain. The constitutive equations without static deformation correction factor cannot describe the peak and anticipate higher dynamic stiffness than the experimental value. The proposed model, however, effectively describes the effects of prestrain that cannot be expressed by conventional constitutive models as shown in the

http://rcin.org.pl

figures. The dynamic stiffness is plotted against the static deformation at 30 Hz in Fig. 14. It is observed that the proposed constitutive model works well at other frequencies. This result confirms the fact that the static deformation correction factor determined at one frequency is also effective at other frequencies in the tested range.

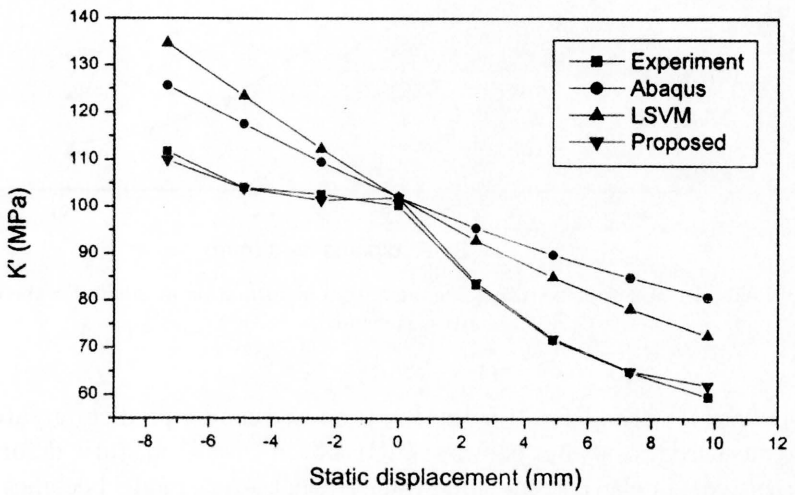

FIG. 12. Real part of complex stiffness against static deformation at 10 Hz for the complex stress specimen.

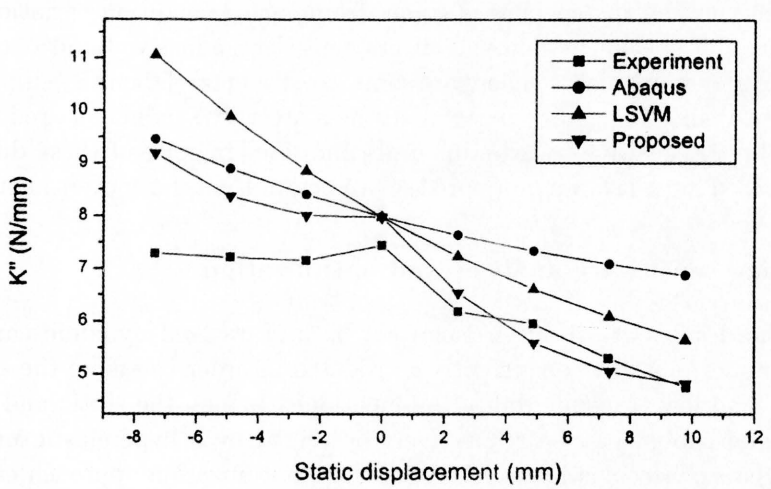

FIG. 13. Imaginary part of complex stiffness against static deformation at 10 Hz for the complex stress specimen.

http://rcin.org.pl

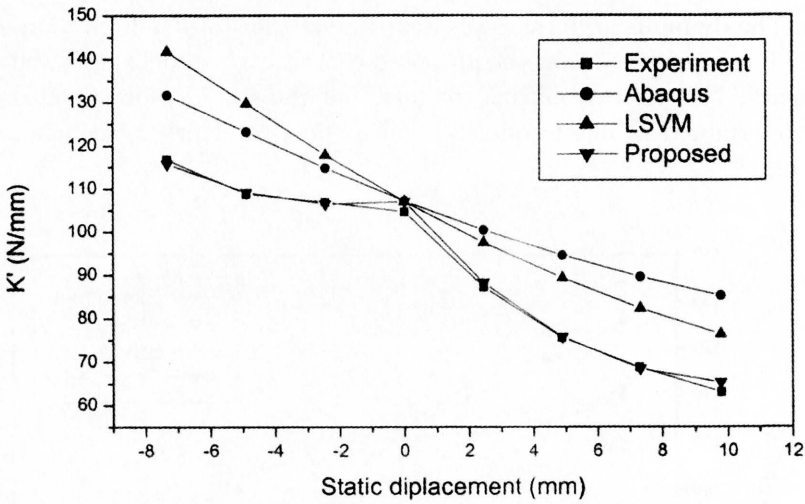

FIG. 14. Real part of complex stiffness against static deformation at 30 Hz for the complex stress specimen.

In prediction of the loss stiffness, the proposed model predicts greater value than the measured result but shows same trend. In case of no static deformation, all constitutive models yield the same value because every model becomes a linear viscoelastic one. The material properties used in the calculation are determined by the uniaxial tension test results. The difference between the computed value and the measured one under no static deformation is caused by material property difference between the test specimens. It is suspected that the material property difference between the specimens comes from curing condition variation during preparation of specimens and the effects caused by adhesive bond between the specimen and fixing plates. There are some experimental difficulties similar to the tension test since imaginary parts of stiffness are very small compared with real part and very sensitive to experimental condition. In spite of these differences, the proposed model shows more precise prediction than the conventional models.

4. Design sensitivity analysis and optimization

In the designs of vibration isolators, both static and dynamic characteristics of rubber must be concurrently considered in order to assure the structural stability and low transmissibility. As mentioned before, the static and dynamic behavior of rubber can be respectively described by a hyperelastic model and a steady-state viscoelastic model. A topology optimization approach can be applied for the shape design of vibration isolator made of filled rubber. For easier application of the optimization algorithm, material property design sensitivity

http://rcin.org.pl

analyses of both the hyperelastic and viscoelastic constitutive equation are developed for topology optimization using the mean compliance and adjoint variables. In order to consider simultaneously the static and dynamic behavior of rubber, a proper topology optimization formulations should be proposed.

4.1. Design sensitivity analysis of the hyperelastic model

The hyperelastic constitutive equation can be written with the following nonlinear energy form and load linear form:

$$a(r,\bar{r}) = l(\bar{r}), \qquad \forall \bar{r} \in U \times P, \tag{4.1}$$

where U and P are spaces of kinematically admissible virtual displacements and hydrostatic pressure, $r = [u_1, u_2, u_3, p]^T$ is the vector of the displacements and hydrostatic pressure. In this equation, each side can be written with integral terms as follows:

$$a(r,\bar{r}) = \delta\left(\int_V {}_0W + {}_0Q dV\right) = \delta\left(\int_V {}_0W - \frac{1}{2KJ_0}(\bar{p}-\hat{p})^2 dV\right), \tag{4.2}$$

$$l(\bar{r}) = {}^t\Re = \int_V f\ u\ dV + \int_S T\ u\ dS, \tag{4.3}$$

where ${}_0W$ represents the energy density function. f and T represent the external volumetric and surface forces.

Material property design sensitivity analysis of hyperelastic model was developed [11]. When a structural system with a given design b is in the final equilibrium configuration at time t, the system reaches another equilibrium at time $t + \Delta t$ due to design perturbation $\tau\delta b$.

$$a_{b+\tau\delta b}(r,\bar{r}) = l_{b+\tau\delta b}(\bar{r}), \qquad \forall \bar{r} \in U \times P. \tag{4.4}$$

Since the difference between the final equilibriums of two designs becomes smaller as design perturbation becomes smaller, the first-order variations of the nonlinear energy form and the linear load form with respect to the design variable can be defined as:

$$a'_{\delta b}(r,\bar{r}) = \frac{d}{d\tau} a_{b+\tau\delta b}(\tilde{r},\bar{r})\bigg|_{\tau=0}, \tag{4.5}$$

$$l'_{\delta b}(\bar{r}) = \frac{d}{d\tau} l_{b+\tau\delta b}(\bar{r})\bigg|_{\tau=0}. \tag{4.6}$$

http://rcin.org.pl

By the chain rule of differentiation, the first order variation of Eq. (4.4) is obtained as:

$$a^*_{\delta b}\left(r; r', \bar{r}\right) = l'_{\delta b}\left(\bar{r}\right) - a'_{\delta b}\left(r, \bar{r}\right). \tag{4.7}$$

Generally, the following static mean compliance can be selected as the static performance measure of the structural system:

$$\psi = \int_V f\, r\, dV. \tag{4.8}$$

If the external force f is independent of the design changes, the first-order variation of the mean compliance is written as follows:

$$\psi' = \int_V f\, r'\, dV. \tag{4.9}$$

Using the adjoint equation, the design sensitivity of static mean compliance is written as:

$$\psi' = -a'_{\delta b}\left(r,\ r\right). \tag{4.10}$$

In this equation, the first order variation of energy form with respect to the design variable can be written in terms related to design variables as follows:

$$a'_{\delta b}\left(r, r\right) = \int_V \delta\varepsilon : \frac{\partial}{\partial \tau}\Big[\mathscr{D}\left(b + \tau\delta b\right)\Big]_{\tau=0} : \varepsilon\, dV + \int_V \frac{\partial}{\partial \tau}\Big[\sigma_0\left(b + \tau\delta b\right)\Big]_{\tau=0} : \Delta\delta_0 E\, dV. \tag{4.11}$$

4.2. Design sensitivity analysis of the steady-state viscoelastic model

Introducing the virtual variable, the complex viscoelastic constitutive equation (2.37) is written as the following energy equilibrium equation:

$$a\left(r^*, \bar{r}^*\right) = \delta W^* = \Delta\Re^* = l\left(\bar{r}^*\right), \qquad \forall \bar{r}^* \in U^* \times P^*, \tag{4.12}$$

where U^* and P^* are spaces of kinematically admissible virtual complex displacements and hydrostatic pressure. The first-order variation of energy equation can be obtained similarly to the static case.

$$a^*_{\delta b}\left(r^*;\, r^{*'}, \bar{r}^*\right) = l'_{\delta b}\left(\bar{r}^*\right) - a'_{\delta b}\left(r^*, \bar{r}^*\right). \tag{4.13}$$

http://rcin.org.pl

In the vibration isolation system, the dynamic performance of the system is the transmissibility from the vibrating systems to the base structures. As shown in Fig. 15 and Fig. 16, the transmissibility of the system has a very similar tendency compared with the dynamic compliance, therefore dynamic compliance can be the dynamic performance measure of structures.

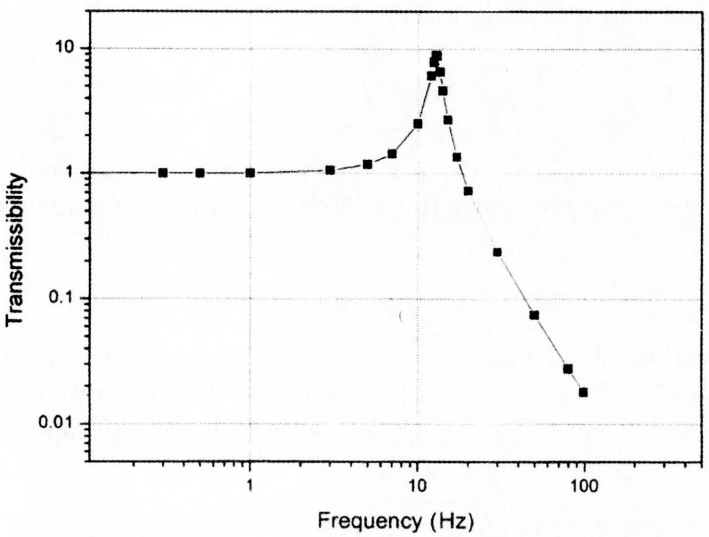

FIG. 15. Transmissibility against vibration frequency.

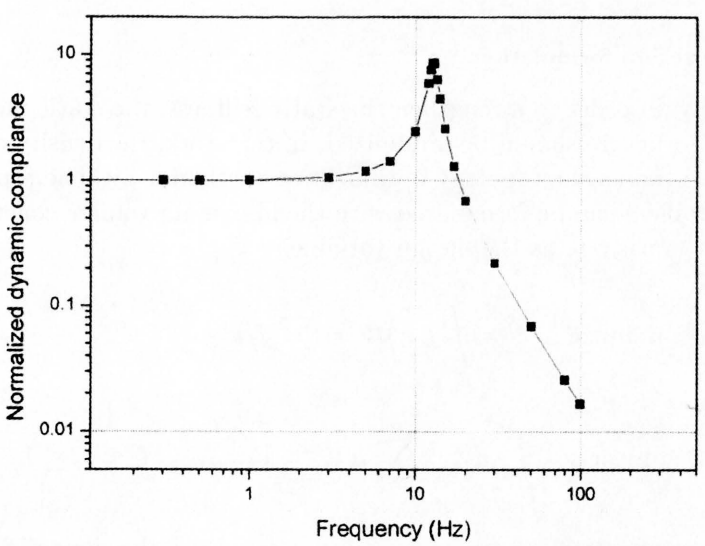

FIG. 16. Normalized dynamic compliance against vibration frequency.

http://rcin.org.pl

The steady-state dynamic compliance can be defined as:

$$\psi^* = \int_V f^* r^* dV. \tag{4.14}$$

If the vibrating external force f^* is independent of the design changes, the first-order variation is obtained as:

$$\psi^{*'} = \int_V f^* r^{*'} dV. \tag{4.15}$$

The design sensitivity of static mean compliance can be written by using the proper adjoint equation similar to the design sensitivity of static mean compliance,

$$\psi^{*'} = -a'_{\delta b}(r^*, r^*). \tag{4.16}$$

In this equation, the dynamic compliance and its first-order variation are the complex variables defined as $\psi^* = (\psi_1 + i\psi_2)$ and $\delta(\psi^*) = (\delta\psi_1 + i\delta\psi_2)$. Therefore, the following two scalar variables can be used as the real-valued performance measure and its design sensitivity.

$$\|\psi^*\| = \sqrt{\psi_1^2 + \psi_2^2}, \tag{4.17}$$

$$\delta\|\psi^*\| = \frac{1}{2}\left(\psi_1^2 + \psi_2^2\right)^{-1/2}\left(2\psi_1\delta\psi_1 + 2\psi_2\delta\psi_2\right). \tag{4.18}$$

4.3. Optimization formulation

Generally, in order to strengthen the static stiffness, the static mean compliance of the structure should be minimized. In this work, the density distribution approach is used as the topology optimization methodology. The topology optimization problem can be formulated with the maximum volume constraint using the element density η_i as the design variable.

$$\begin{aligned} &\text{minimize} \quad \psi = \int_V f\ r\ dV = \sum_j^{N_f} f_j u_j, \\ &\text{subject to} \quad \int_V \eta dV = \sum_i^{nel} \eta_i V_i^e \le V_{\max}, \qquad 0 \le \eta_i \le 1. \end{aligned} \tag{4.19}$$

In the optimization for transmissibility, we can use the dynamic compliance as the objective function and then the optimization problem can be formulated as

http://rcin.org.pl

follows. In order to minimize the transmissibility, the dynamic mean compliance should be minimized. The volume constraint must be reversed to minimum value because the structure will become very flexible in view of low force transmission.

$$\begin{aligned} &\text{minimize} \quad \psi = \|\psi^*\| = \left\| \int_V f^* r^* \, dV \right\| = \left\| \sum_j^{N_f} f_i^* u_i^* \right\|, \\ &\text{subject to} \quad \int_V \eta \, dV = \sum_i^{nel} \eta_i V_i^e \geq V_{\min}, \quad 0 \leq \eta_i \leq 1. \end{aligned} \tag{4.20}$$

In order to make an isolator endure the static loadings and reduce the force transmission, the static and dynamic compliance of the structure should be simultaneously considered. Multi-objective optimization can be used for this problem, but the sensitivity differences of static and dynamic compliance cause some difficulties. In this paper, the dynamic compliance is minimized with the maximum static compliance constraint as well as the volume constraint. Such topology optimization problem can be formulated as:

$$\begin{aligned} &\text{minimize} \quad \psi = \|\psi^*\| = \left\| \int_V f^* \, r^* \, dV \right\| = \left\| \sum_j^{N_f} f_i^* u_i^* \right\|; \\ &\text{subject to} \quad h_1 = \int_V f \, r \, dV - C_{\max} = \sum_j^{N_f} f_i u_i - C_{\max} \leq 0, \\ &\qquad h_2 = \int_V \eta \, dV - V_{\max} = \sum_i^{nel} \eta_i V_i^e - V_{\max} \leq 0 \, , \\ &\qquad h_3 = V_{\min} - \int_V \eta \, dV = V_{\min} - \sum_i^{nel} \eta_i V_i^e \leq 0, \\ &\qquad 0 \leq \eta_i \leq 1. \end{aligned} \tag{4.21}$$

As mentioned before, the density distribution approach is selected and the design densities indicating the material existence are used as design variables. In order to assure the existence and uniqueness of a solution, a relaxed and penalized artificial material model is selected. The relation between the elastic modulus and the design density in this artificial material model is represented by the following equation and its characteristics are presented in Fig. 17. As parameter α increases, the relation becomes more penalized.

http://rcin.org.pl

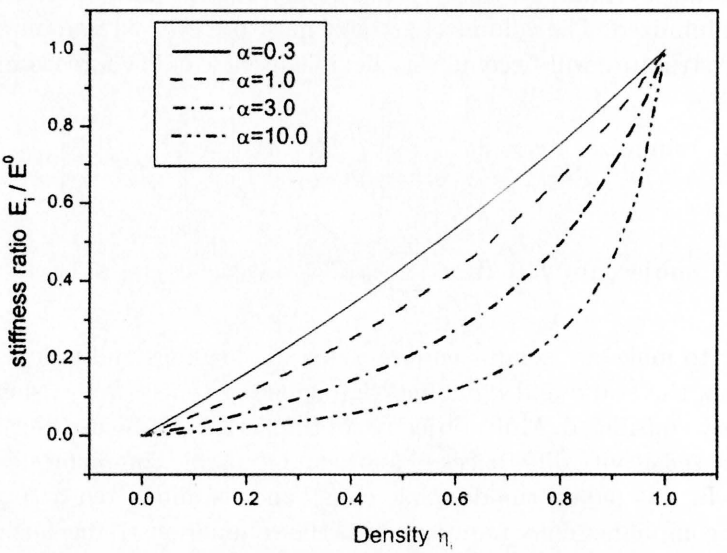

FIG. 17. Characteristics of artificial material model.

$$E_i = \frac{\eta_i}{1 + \alpha(1 - \eta_i)} E_i^0. \tag{4.22}$$

In this work, the three-dimensional quadratic hybrid elements are used in FE analysis for each static and steady-state dynamic problem. The hybrid elements have 27 displacement-nodes and 4 hydrostatic pressure degrees of freedom for the treatment of incompressible or nearly incompressible behavior. Therefore the locking phenomena and checkerboard pattern can be effectively removed. And also the continuation methods for volume and static compliance constraints are used in order to prevent the local minima. A sequentially linear programming (SLP) algorithm is selected as the optimization algorithm, which updates the design variable to improve the performance of structures.

5. Design examples

A simple structure shown in Fig. 18 is selected as a numerical example to demonstrate this approach. A natural rubber filled 70 phr carbon black is applied as the isolator material and steel (ASTM A36) is selected as a non-design mass material. A mass to be isolated is located on the top center surface of rubber. A large static deformation is generated by self-weight of the mass and external vibrating forces are vertically applied to the mass center. The volume constraint for design is set to 50% for all following problems.

http://rcin.org.pl

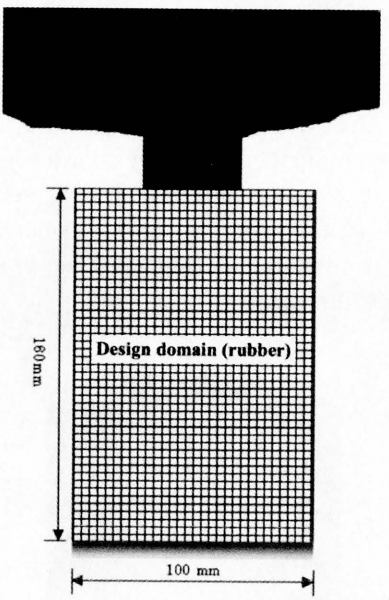

FIG. 18. Schematic diagram of simple structure problem ($t = 10\,\text{mm}$).

At first, the static design result for minimizing the static compliance and obtaining the highest stiffness is shown in Fig. 19. A very stiff structure within the given volume constraint was obtained and this structure is strong enough to endure the large static load. For the design problem to minimize the transmis-

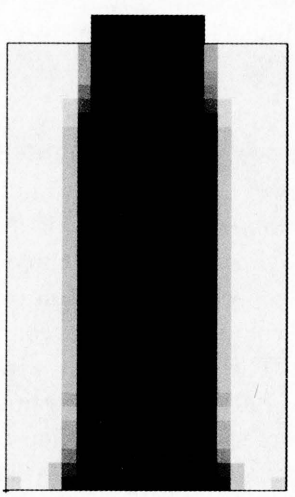

FIG. 19. Maximum static stiffness design of simple structure problem.

http://rcin.org.pl

sibility for 20 Hz vibrating frequency, a very flexible structure is obtained and shown in Fig. 20. This structure has a very small natural frequency and shows very low transmissibility, however it is too weak to endure the self-weight of the mass. It is obvious that the static stiffness compared to the mass is very small because of a large cavity under the mass. If this design is applied for isolator, very large static deformations may be generated by self-weight of mass and the structure may become unstable due to small disturbances. Therefore it is impossible that the design results considering only the dynamic behavior of rubber could be applied to vibration isolator.

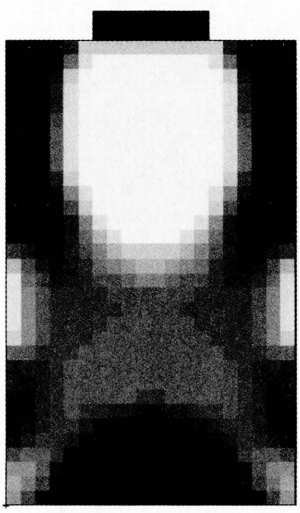

FIG. 20. Minimum transmissibility design of simple structure problem ($f = 20$ Hz).

For this reason, the static and dynamic behavior of rubber must be simultaneously considered in the design process of anti-vibration rubber. A topology optimization process to minimize the dynamic compliance with the static compliance constraint as well as volume constraint is attempted. During iteration of the optimization, structure may become flexible in order to minimize the dynamic compliance and then a large deformation occurs with the element distortions. The continuation of volume and static constraints is applied to avoid this mesh-distortion problem. The design result within 120% static constraint is represented in Fig. 21. The 120% static constraint means that the structure can be deformed within 120% of static deformation of maximum static stiffness design. The obtained result shows a complex truss-like structure. As represented in Table 3, this structure has a sufficient stiffness for static loading by the mass and shows about 20% lower transmissibility compared to the static stiffness de-

http://rcin.org.pl

sign. On the contrary, the static deformation due to static loading increases by about 20%. We can conclude that the proposed design method is effective for vibration isolator design.

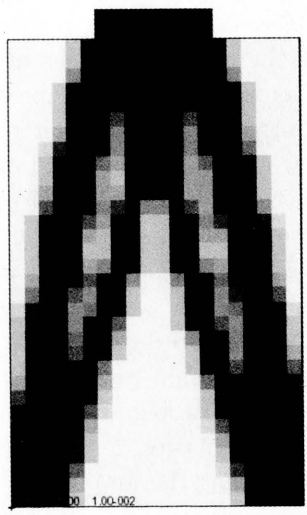

FIG. 21. Simultaneous design result of simple structure problem ($f = 20$ Hz, 120% static compliance constraint).

Table 3. Design results of simple structure problem.

Design method	Static design	Dynamic design	Simultaneous design
Static compliance	0.1990635E+00	Not available	0.2401379E+00
Transmissibility	0.1577919E+00	0.2596466E–02	0.1262678E+00
Dynamic compliance	0.1181939E–05	0.1030806E–05	0.1151566E–05

6. Conclusions

A constitutive model, FE formulation and topology optimization for rubber that is under small oscillatory loads superimposed on large static deformation was discussed. The constitutive model was proposed and implemented in a finite element code to calculate the behavior of rubber under complicated loading conditions. Updated Lagrangian formulation with displacement–pressure mixed

http://rcin.org.pl

method was used to treat the incompressible large deformation problem. Dynamic tests under specified loading conditions were executed in order to verify the proposed constitutive model. Complex stress-state tests are included in the dynamic tests to verify the model under multi-axial stress states. The results computed by the FEA code were compared with the test results to estimate the performance of the model. In the complex stress-state test, it is clearly observed that the undeformed state is expressed as a local maximum point in the dynamic stiffness plot. The proposed model successfully predicts the peak point and its computed results agree well with the experimental ones.

For the stability and low transmissibility of isolation systems, a topology optimization method was proposed considering both the static and dynamic performance. Material property design sensitivity analysis of the hyperelastic model and steady-state viscoelastic one were developed using the mean compliance and adjoint variables. A simple design example was presented and design results showed that the proposed design process could simultaneously consider the static and dynamic behavior of rubber with adequate constitutive models.

The amplitude of dynamic deformation generally affects the dynamic stiffness (Payne effect). It is anticipated that the amplitude effects increase with larger strain amplitude and amplitude variation. As a future work, we are now trying to include the Payne effect in our constitutive equation and consider more realistic loading conditions for the isolator design.

Acknowledgment

This work was supported by grant No.R01-2001-000-00393 from the Basic Research Program of the Korea Science & Engineering Foundation.

References

1. J. I. SULIVAN, K. N. MORMAN and R. A. PETT, *A non-linear viscoelastic characterization of a natural rubber gum vulcanizate*, Rubber Chemistry and Technology, **53**, 805–822, 1980.

2. K. N. MORMAN Jr and J. C. NAGTEGAAL, *Finite element analysis of sinusoida small-amplitude vibrations in deformed viscoelastic solids. Part I: theoretical development*, International Journal For Numerical Methods in Engineering, **19**, 1079–1103, 1983.

3. A. B. ZDUNEK, *Theory and computation of the steady state harmonic response of viscoelastic rubber parts*, Computer Methods in Applied Mechanics and Engineering, **105**, 63–92, 1993.

4. A. B. ZDUNEK, *Determination of material response functions for prestrained rubbers*, Rheologica Acta, **31**, 575–591, 1992.

5. HIBBIT, KARLSSON and SORENSON INC., *ABAQUS theory manual*, Version 5.7. 997.

http://rcin.org.pl

6. A. VOET and J.C. MORAWSKI, *Dynamic mechanical and electrical properties of vulcanizates at elongations up to sample rupture*, Rubber Chemistry and Technology, **47**, 765–777, 1974.

7. P. MASON, *The viscoelastic behavior of rubber in extension*, Journal of Applied Polymer Science, **1**, 1, 63–69, 1959.

8. O. KRAMER, S. HVIDT and J.D. FERRY, *Dynamic mechanical properties*, [in:] J.E. MARK *et al.* [Ed.] Science and Technology of Rubber, Academic Press, San Diego 1994.

9. B.K. KIM and S.K. YOUN, *A viscoelastic constitutive model of rubber under small oscillatory loads superimposed on large static deformation*, Archive of Applied Mechanics, **71**, 11, 748–763, 2001.

10. Y. YU, N.G. NAGANATHAN and R.V. DUKKIPATI, *A literature review of automotive vehicle engine mounting systems*, Mechanism and Machine Theory, **36**, 123–142, 2001.

11. K.K. CHOI and W. DUAN, *Design sensitivity analysis and shape optimization of structural components with hyperelastic material*, Computer Methods in Applied Mechanics and Engineering, **187**, 219–243, 2000.

12. J.J. KIM and H.Y. KIM, *Shape design of an engine mount by a method of parameter optimization*, Computers and Structures, **65**, 5, 725–731, 1997.

13. S.H. KI and S.M. WANG, *Topology optimization of hyperelastic material*, Proceedings of 4th world congress of structural and multidisciplinary optimization, June 4-8 2001, Dalian, China.

14. J.C. SIMO, *A fully three-dimensional finite-strain viscoelastic damage model: formulation and computational aspects*, Computer Methods in Applied Mechanics and Engineering, **60**, 153–173, 1987.

15. R.M. CHRISTENSEN, *Theory of viscoelasticity*, Academic Press, New York 1982.

16. C. TRUESDELL and W. NOLL, *The nonlinear field theories of mechanics*, [in:] Encyclopedia of Physics, S. FLÜGGE [Ed.], Springer-Verlag, New York 1965.

17. G D. JUNG, S.K. YOUN and B.K. KIM, *A three-dimensional nonlinear viscoelastic constitutive model of solid propellant*, International Journal of Solids and Structures, **37**, 4715–4732, 2000.

18. T. SUSSMAN and K.J. BATHE, *A finite element formulation for nonlinear incompressible elastic and inelastic analysis*, Computers & Structures, **26**, 1/2, 357–409, 1987.

19. R.P. BROWN, *Physical testing of rubber*, Chapman & Hall, London, 3rd [Ed.], 1996.

Received December 5, 2002; revised version July 25, 2003.

http://rcin.org.pl